Al Azhar Bulletin of Science Vol. (26) No.2, December, 61-84, 2015.

SEDIMENTOLOGICAL, PETROGRAPHICAL AND GEOCHEMICAL CHARACTERIZATION OF THE OLIGOCENE "GABAL AHMAR FORMATION" AT MAADI-QATTAMIYA AREA, EGYPT

ELSHAHAT O.R.

Geology Department, Faculty of Science, Al-Azhar University

ABSTRACT

An integrated mechanical, mineralogical, petrographical and geochemical studies were carried out on the sand and sandstone samples from the Gabal Ahmar Formation in Maadi- El Qattamiya area. Twenty-nine samples were collected from two sections. Grain size analysis of the studied sediment has been carried to evaluate its textural parameters and statistical measures to depict the depositional pattern of sediments in the study area.

The samples are medium to very coarse-grained (1.007 to -0.54 φ), poorly to very well-sorted (-0.040 to 1.32φ), very fine to coarse skewed (-0.11 to 1.72φ) and mesokurtic to very leptokurtic (-1.59-2.82φ) in nature. The grain size distribution reveals that the transporting medium must have undergone series of rise and fall in its velocity. The studied samples could be classified into three types gravelly and slightly gravel sand, gravel and sand class.

Petrographically, the Gabal Ahmar sandstones are mainly ferruginous arenite, ferruginous and calcareous greywackes, generally, moderately/poorly sorted, sub-angular, sub-rounded with silica, carbonate and sericite cement. The main mineralogical constituents are quartz, montmorillonite, calcite, microcline and hematite. The detected heavy minerals are magnetite, hematite, limonite, zircon, and glauconite. All the identified grains of heavy minerals show different shapes.

The geochemistry of the studied sandstones supports the petrographic results. The sandstone is therefore highly siliceous, with exception of three calcareous sandstone samples which recorded a major amount of CaO up to 30.35%. The Gabal Ahmar sandstones can be classified chemically into arenite and greywacke.

Keywords: Grain size analysis, depositional environment, heavy minerals, geochemical analysis, Gabal Ahmar Formation.

1.INTRODUCTIN

Grain size analysis has been widely used to statistically exa mine sp atial v ariation in sediment size properties. It was pioneered by Mclaren (1981). Recent applications include the studies by Jitheshkumar et al. 2013, Balsinha et al. 2014, Garwood et al. 2015 and Ordóñez et al. 2016.The study of grain size remains significant in the understanding of transport process pattern because grain-size trends seem to be the natural result of dy namic s ediment t ransport p rocesses (Vandenberghe 2013). The application of extended and multivariate statistical analyses of grain size distributions are effective at identifying discrete s imilarities and differences between mixed sediment populations (Nelson et al., 2014).

The Maadi- Qattamiya area occurs in the eastern part o f C airo in the Maad i–Qattamiya Road East of Greater Cairo and west of Gulf of Suez. These parts of Eastern Desert represent the uns table s helf un its, w hich c omprise t he greater part of northern Egypt (Said 1962). The study area is covered essentially by sedimentary rocks with limited Tertiary basaltic flow sheets.

The O ligocene deposits are w idely di stributed in the Cairo-Suez district. They cover a long tract of desert from northeast of Cairo to Anqabia, a nd form sev eral pa tches t o the sout h and north of the asphaltic road. T he sediments are mainly c omposed of s and and gravel w ith l arge trunks and fragments of silicified wood and basalt flows and dykes. The volcanic rocks are believed by different authors, to be Tertiary (Oligocene) based on their field relations (Said, 1962).

2. GEOLOGICAL SETTING

The st udy ar ea c omprises di fferent t opographic un its i ncluding: p lateaux, w adis, l owland a nd i solated hills. M ost l ow l ands a re be longing to the Upper Eocene rocks while others are be longing t o t he O ligocene s ands, g ravels, quartzite and basaltic rocks.

Structurally; the s tudied district is related to the tectonics of the Gulf of Suez and appear that nearly all the heights bounded by fault sets. The structural f eatures d escribed carefully by Moustafa et al., (1991). T he exposed rocks are affected by nor mal f aults in a ddition t o few of folds and joints. The faults of the east-west set

affect the Oligocene and Miocene rock units, which exposed at the northeastern part of the studied district, the faults of the northwest-southeast set dissect the Eocene rocks in the northern and southern parts of the studied district in addition to the Oligocene and Miocene rocks in its northwestern part.

The Oligocene sediments are represented by sand and gravels (Gabal Ahmar Formation) and basaltic flows unconformably overlies the Upper Eocene rocks. The Oligocene sediments are mainly composed of loose or weakly consolidated sand and gravel with large trunks of silicified wood. The sediments exhibit cross stratification, which is highly illustrated by the changing of colors, reddish brown, brownish yellow and black. Therefore, hard cement sandstone is common in certain places, especially near fault planes due to uprising silica and iron bearing fluids. The sediments truncated by the faults usually imparted by red, yellow and brown colorations because of staining by iron oxy-hydroxides.

Gabal Ahmar Formation covered by weathered basaltic rocks of pale grey color (reaching 30m) in many parts of the studied area. Silicification and multi-ferrugination occur along fissures, joints and fault planes due to hydrothermal solutions accompanying the extrusion of basalt, during the Oligocene volcanicity in our study area.

Stratigraphic section at Tolba Quarry

This section was measured at latitude 290 36' 23'' N and longitude 310 55' 05'' E. It attains 11.67m thickness (Fig.1). At this section, the Gabal Ahmar Formation is represented by alternation of vary colored (pale red to red), friable, fine to coarse grained slightly calcareous and highly ferruginous, with vary amount of gravels. These gravels are reddish and black, rounded to angular, spherical to rod shape, with different size (up to 12 cm). Yellow siltstone bed is present. The sequence is topped by basaltic flows (Figs. 3, 4 &5).

Stratigraphic section at Naqb Ghul area

This section was measured at the south part of Naqb Ghul area at latitude 290 35' 43'' N and longitude 310 54' 08 '' E and attains 8.1m thickness. The sequence is divided into 14 beds according to the color of sand and the presence or absence of gravels (Fig. 2). Lithologically this sequence consists essentially of highly ferruginous, vary colored (yellow at the base and pale red to red at the top), friable, fine to coarse grained sands with vary amount of gravels (reddish and black), sometimes fractured, rounded to angular, spherical to rod shape, with different size (up to 13 cm). Siltstone (grey with pale red staining), bed is also represented in this section. The upper part is made up of basaltic rocks which are covering this sequence (Figs.6 &7).

3. MATERIALS AND METHODS

A total of thirty sand and gravels and sandstone samples representing the Gabal Ahmar Formation had been collected from two sections around Maadi-Qattamiya area. Grain-size analysis for twenty- seven samples (about 500 grams) were subjected to dry sieving analysis using Folk and Ward methods (1957) to detect the different textural parameters and the sedimentary environment. Estimation of the grain- size parameters were carried out using of GRADISTAT program (Blott and Pye, 2001). The fine and very fine (0.125 -0.073 mm) sand fractions selected ten samples were separated into light and heavy minerals using bromoform. The heavy fractions are passed through a hand magnetic separator to capture the magnetic fractions.

Microscopic examination and counting of both heavy and light fractions, whereas, more than 500 grains for each sample are counted to detect their concentration and distribution. Moreover, nine samples were selected to petrographic and geochemical examination to detect the microfacies associations and the major and trace element distribution. Ten bulk samples were powdered for X-ray diffraction analysis for identification the main mineral composition.

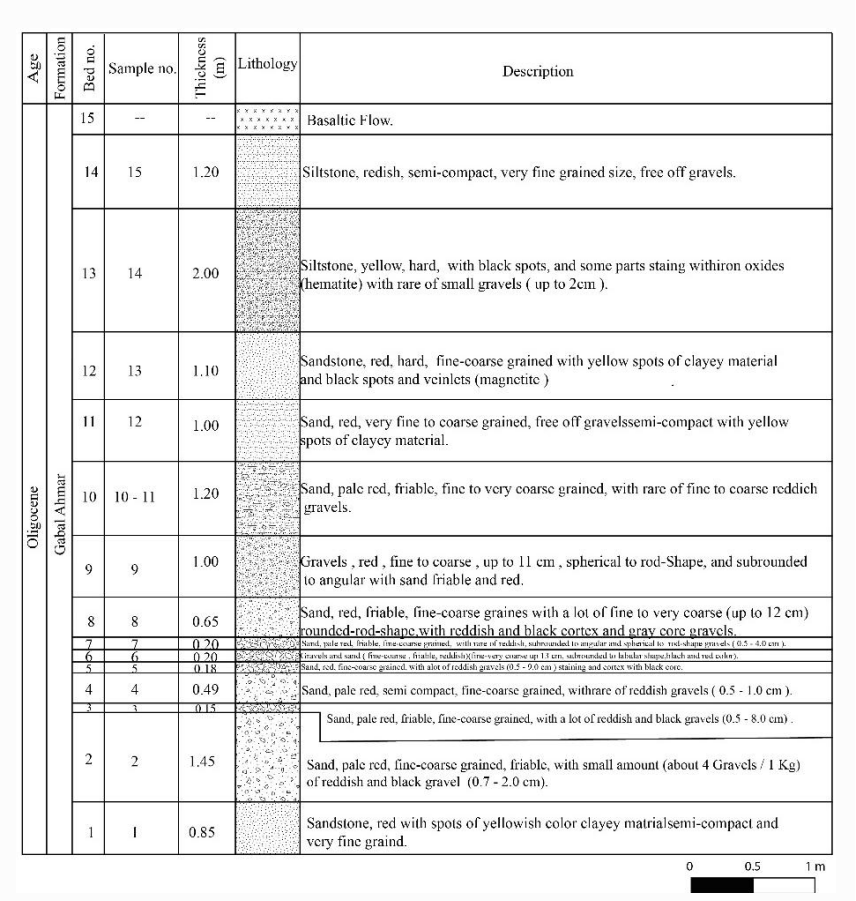

Fig. 1: Stratigraphic columnar section of the Gabal Ahmar Formation at Tolba Quarry section.

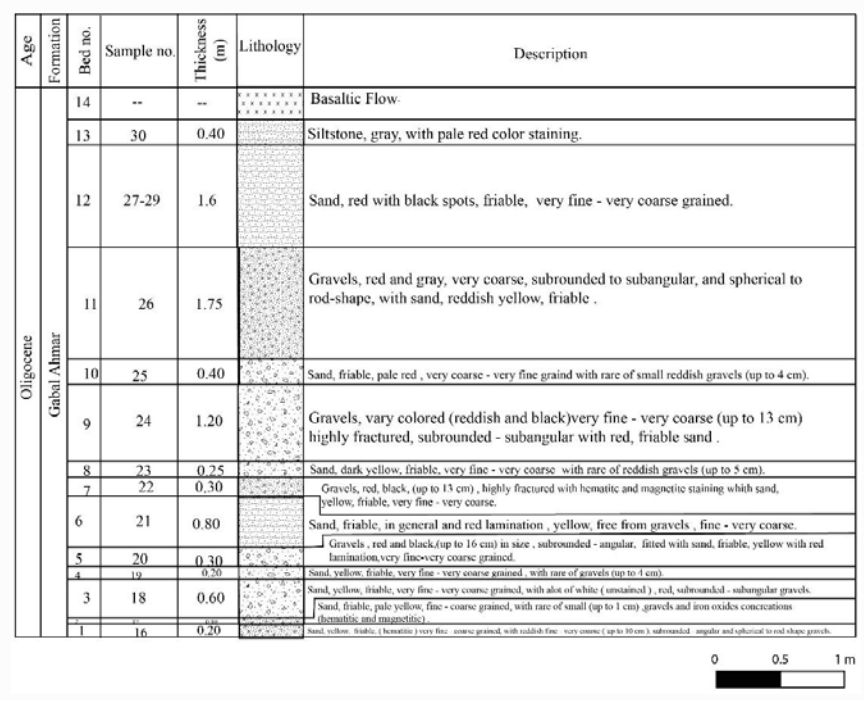

Fig. 2: Stratigraphic columnar section of the Gabal Ahmar Formation at Naqb Ghul section.

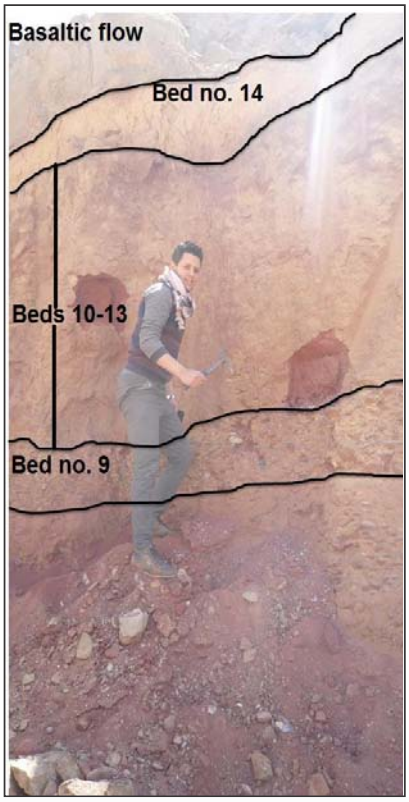

Fig. 3: Photograph showing sedimentary sequence at Tolba quarry section, beds 9-14.

Fig. 4: Photograph showing pale red, friable, fine to coarse grained sand with rare of vary size, red gravels, samples no. 10&11.

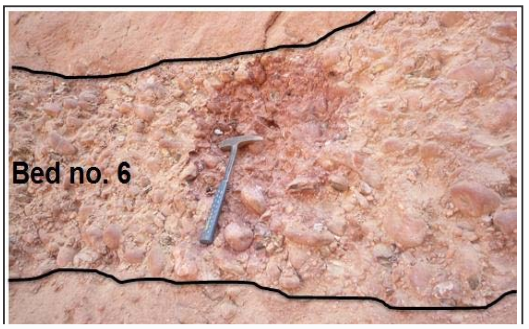

Fig. 5: Photograph showing fine-very coarse (up to 13cm), sub-rounded to sub-angular, spherical to rod shape red color gravels, sample no. 6.

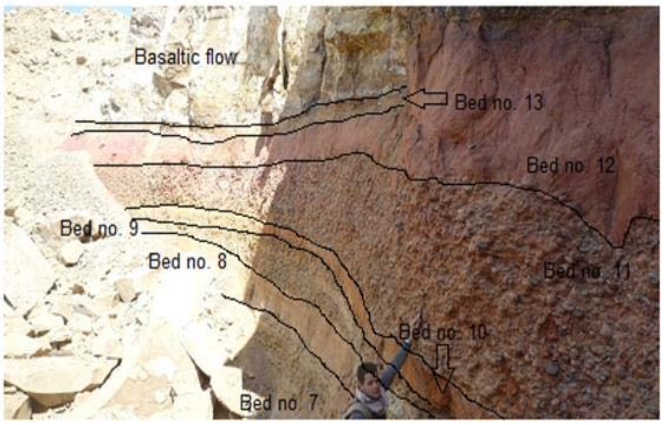

Fig. 6: Photograph showing sedimentary sequence at Naqb Ghul section, beds 7-13.

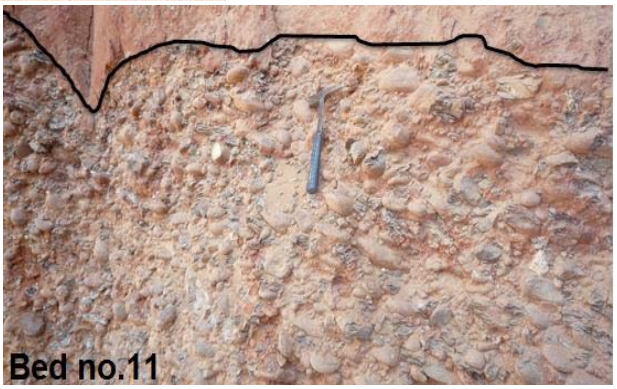

Fig. 7: Photograph showing ill sorted, fractured, sub-rounded to sub-angular, spherical to rod shape red and grey color gravels, sample no. 26.

4. RESULTS AND DISCUSSIONS

4.1. Grain size analysis

After the samples have been dried, sieve analysis was carried out for twenty- seven samples. Sieving technique is applied to separate the grains of various size-classes, as proposed by Ingram (1971). Grain size data of the studied samples are presented graphically in the form of histograms, frequency and cumulative frequency curves. For determination of grain size parameters, cumulative frequency curves were drawn on arithmetic probability papers. Statistical graphic measures such as graphic mean size (Mz), unclusive graphic standard deviation (δ1), inclusive graphic skewness (Sk1) and the graphic kurtosis (KG) were calculated using Folk and Ward (1957) and the data were presented in Table (1). It is clear from the reprehensive histograms that the examined grain-size is related to unimodal and bimodal type samples, meanwhile the majorities are unimodal (21 samples) as shown in figure (8). Bimodality may be due to the mixing of two different populations or either high strength of floods and short duration of deposition, or the increasing power of wave generated by wind along beach (Pettijohn 1975).

Frequency curves of the studied samples show that most of the studied sediments are unimodal with two dominant size-class: coarse and medium sands (Fig. 10). Frequency curves show positive, negative as well as nearly symmetrical distribution. Such highly variable nature of the frequency curves indicates fluctuation in the energy condition at the time of deposition of these sediments.

The mean size indicates a measure of central tendency or the average size of the sediment. Translated in terms of energy, it indicates the average kinetic energy (velocity) of the depositing agent (Sahu 1964). The mean size in the examined samples vary from 1.007 to -0.542Φ, indicating medium to very coarse sands which, indicates the variation in the kinetic energy at the time of deposition (Amaral and Pryor, 1977) or it could suggest that the grains were derived from different sources.

The results show that; the sand size ranges from 4.7% to 97.8%, gravel ranges from 0.1% to 91.8% while silt and clay ranges from 0.1% to 5.8%. The studied samples could be classified according to Blair and Mc Pherson (1999) into three types (Fig. 11) going very well with the classification based upon histograms (Fig. 8) and cumulative curves (Fig. 9). The first type of collected sediments is composed of admixture of gravel and sand at different ratios; they are classified as gravelly and slightly gravel sand (13 samples). The second type of sediments is characterized by considerable gravel content; it includes gravel and sand gravel (11 samples). The third type of sediments is composed entirely of sand and is classified as sand class (3 samples).

The wide range of grain size in most of the analyzed samples demonstrates poorly and moderately sorting reflecting the variable velocities and increasing the sedimentation rate.

On the other hand, the stander deviation (σI) was calculated according to (φ84-φ16 /4 + φ95-φ5 /6.6). Sorting deduced for the samples ranges from -0. 040 φ to 1.32φ (poorly sorted 15 samples, moderately sorted 3 samples, moderately well sorted two samples and very well sorted 7 samples). Generally, the gravelly sands are poorly sorted as a result of mixing of sand mode with gravel mode.

Moreover, the skewness values (Sk1) calculated as (φ16 + φ84 - 2φ50)/2(φ84-φ16) + (φ95+φ5 + 2φ50)/ 2(φ95-φ5) are ranging from (-0. 11 φ to 1.72 φ). In case of skewness, out of total samples 12 are very fine skewed, 4 are fine skewed, 9 are symmetrical and only 2 samples are coarse skewed. Fine tail distribution is more common that suggest high kinetic energy of the depositional basin (Devi 2014). It is observed that most of the studied sand samples possess positive skewness values, the predominance of gravelly and coarse sediments led also to positive skewness. It is observed that some samples possess negative skewness values (coarse tailed),

especially those characterized by high-energy conditions. This resulted in the removal of the fine particles by winnowing action of waves and currents (Temitope 2016).

The calculated kurtosis values (KG) are ranging from -1.59 φ to 2.82 φ. With respect to the kurtosis, on the average the samples are describes as mesokurtic, but some platykurtic to very platykurtic or leptokurtic to very leptokurtic curves could also be observed.

In order to discriminate the depositional processes and environments of the sand and gravels samples, the bivariate scatter plots as suggested by Moiola and Weiser (1968) have been used in the present analysis (Fig. 12). Bivariate plots of the studied samples indicate that most of the samples falls in the field of beach while others within the field of fluvial environment, reveals that these sediments were deposited under diverse conditions by different process. Analysis of data generated from the discriminant functions proposed by Sahu (1964) reveals that the studied samples were deposited under diverse conditions; the most samples indicate beach (25 samples), turbidity current (23 samples) and shallow agitated (21 samples) while four samples indicate fluviatile environment.

Cumulative curves plotted on the probability ordinate scale do not form continuous straight line (Fig. 9). The most samples curves show two, three or more straight line segments. Each segment has different slope which indicates the presence of more than one population of grains or suggest the mixing of detritus carried by currents with different energy (Sharda and Verma 1977). Each of this population is related to different mode of transportation-traction, saltation and suspension (Doeglas, 1946; Visher, 1969 and Moss, 1962 and 1963).

It is observed that the sediments in the study area range from fine sand to coarse sand. This shows that the transporting agent must have undergone several stages of rise and fall. For fine sediments to be deposited in an environment, low energy of the transporting medium is required. However, for coarse grained sediments to be transported, a high transporting energy is required to transport the sediment from its initial state to its current state. Therefore, it can be inferred from the aforementioned statement that the finer sand particles must have been transported when the transporting medium velocity was low, while the coarser sand must have been deposited when the energy of the transporting medium was high. The transporting medium must have undergone series of changing in its velocity. In sediments with bimodal histogram (Fig.8), two flow regimes are suggested, while sediments with unimodal histogram, a single flow regime are suggested.

By applying Zingg form index (1935) on the studied gravels (about 27 units per sample), the average form of the studied gravels is oblate (8 samples), spherical (5 samples), prolate (2 samples) and one sample is triaxial (Fig. 13a), all gravels are staining with iron oxides (hematite and limonite), (Fig. 13b).

4.2 Petrography and Mineralogy

4.2.1Petrograpgy

The petrographic investigation of the Gabal Ahmar selected sandstone samples indicates that they are mainly ferruginous arenite, ferruginous and calcareous greywackes. The Gabal Ahmar sandstones are generally, moderately/poorly sorted, sub-angular, sub-rounded. The main mineralogical constituents are quartz, calcite (micrite and sparite) and iron oxides.

a. Ferruginous quartz-arenite facies

This microfacies associations is composed of quartz grains ranging from about (up to 90 %), they are coarse to medium in size and occasionally fine grains, quartz grains are sub-rounded to sub-angular in shape, sometimes rounded, and texturally ranged from immature to sub-mature which indicates short transportation and immature sediments, they are poorly sorted. It is commonly occurred as monocrystalline quartz with normal and wave extinction and rarely polycrystalline. The cementing materials are mostly of silica and iron oxides (Fig. 14).

Table.1: The grain size parameters of the studied sand samples following Folk and Ward (1957).

S. No.	Sample type	Textural group	Folk and Ward method (description)		
			Mean (Mz)	Skewness (SK_I)	Kurtosis (K_G)
1	Bimodal, Poorly Sorted	Slightly Gravelly Sand	Medium Sand	Very Fine Skewed	Leptokurtic
2	Unimodal, Poorly Sorted	Gravelly Sand	Medium Sand	Symmetrical	Leptokurtic
3	Unimodal, Moderately Sorted	Sandy Gravel	Coarse Sand	Very Fine Skewed	Mesokurtic
4	Unimodal, Moderately Sorted	Sand	Medium Sand	Symmetrical	Mesokurtic
5	Unimodal, Moderately Well Sorted	Sandy Gravel	Very Coarse Sand	Very Fine Skewed	Leptokurtic
6	Unimodal, Very Well Sorted	Sandy Gravel	Very Coarse Sand	Very Fine Skewed	Very Platykurtic
7	Unimodal, Poorly Sorted	Slightly Gravelly Sand	Medium Sand	Symmetrical	Leptokurtic
8	Bimodal, Moderately Well Sorted	Sandy Gravel	Very Coarse Sand	Very Fine Skewed	Very Leptokurtic
9	Unimodal, Very Well Sorted	Gravel	Very Coarse Sand	Symmetrical	Platykurtic
10	Unimodal, Poorly Sorted	Sand	Coarse Sand	Fine Skewed	Platykurtic
11	Bimodal, Poorly Sorted	Sand	Medium Sand	Fine Skewed	Mesokurtic
12	Unimodal, Poorly Sorted	Slightly Gravelly Sand	Medium Sand	Fine Skewed	Leptokurtic
15	Bimodal, Poorly Sorted	Slightly Gravelly Sand	Medium Sand	Very Fine Skewed	Mesokurtic
16	Bimodal, Very Well Sorted	Gravel	Very Coarse Sand	Very Fine Skewed	Very Platykurtic
17	Unimodal, Poorly Sorted	Gravelly Sand	Medium Sand	Fine Skewed	Mesokurtic
18	Unimodal, Very Well Sorted	Gravel	Very Coarse Sand	Very Fine Skewed	Very Platykurtic
19	Unimodal, Poorly Sorted	Gravelly Sand	Medium Sand	Symmetrical	Leptokurtic
20	Unimodal, Very Well Sorted	Gravel	Very Coarse Sand	Very Fine Skewed	Very Platykurtic
21	Unimodal, Poorly Sorted	Slightly Gravelly Sand	Medium Sand	Symmetrical	Leptokurtic
22	Unimodal, Moderately Sorted	Sandy Gravel	Coarse Sand	Very Fine Skewed	Very Platykurtic
23	Unimodal, Poorly Sorted	Gravelly Sand	Medium Sand	Coarse Skewed	Mesokurtic
24	Unimodal, Very Well Sorted	Gravel	Very Coarse Sand	Very Fine Skewed	Very Platykurtic
25	Unimodal, Poorly Sorted	Gravelly Sand	Medium Sand	Coarse Skewed	Mesokurtic
26	Bimodal, Very Well Sorted	Gravel	Very Coarse Sand	Very Fine Skewed	Very Platykurtic
27	Unimodal, Poorly Sorted	Slightly Gravelly Sand	Medium Sand	Symmetrical	Mesokurtic
28	Unimodal, Poorly Sorted	Slightly Gravelly Sand	Medium Sand	Symmetrical	Mesokurtic
29	Unimodal, Poorly Sorted	Slightly Gravelly Sand	Medium Sand	Symmetrical	Mesokurtic

	Mean (Mz)	**Skewness (SK_I)**	**Kurtosis (K_G)**	**Standard deviation (St. dev.)**
Min.	-0.02	-0.02	-0.04	-0.17
Max.	1.57	1.73	2.82	1.32
Avg.	0.74	0.845	1.37	0.49

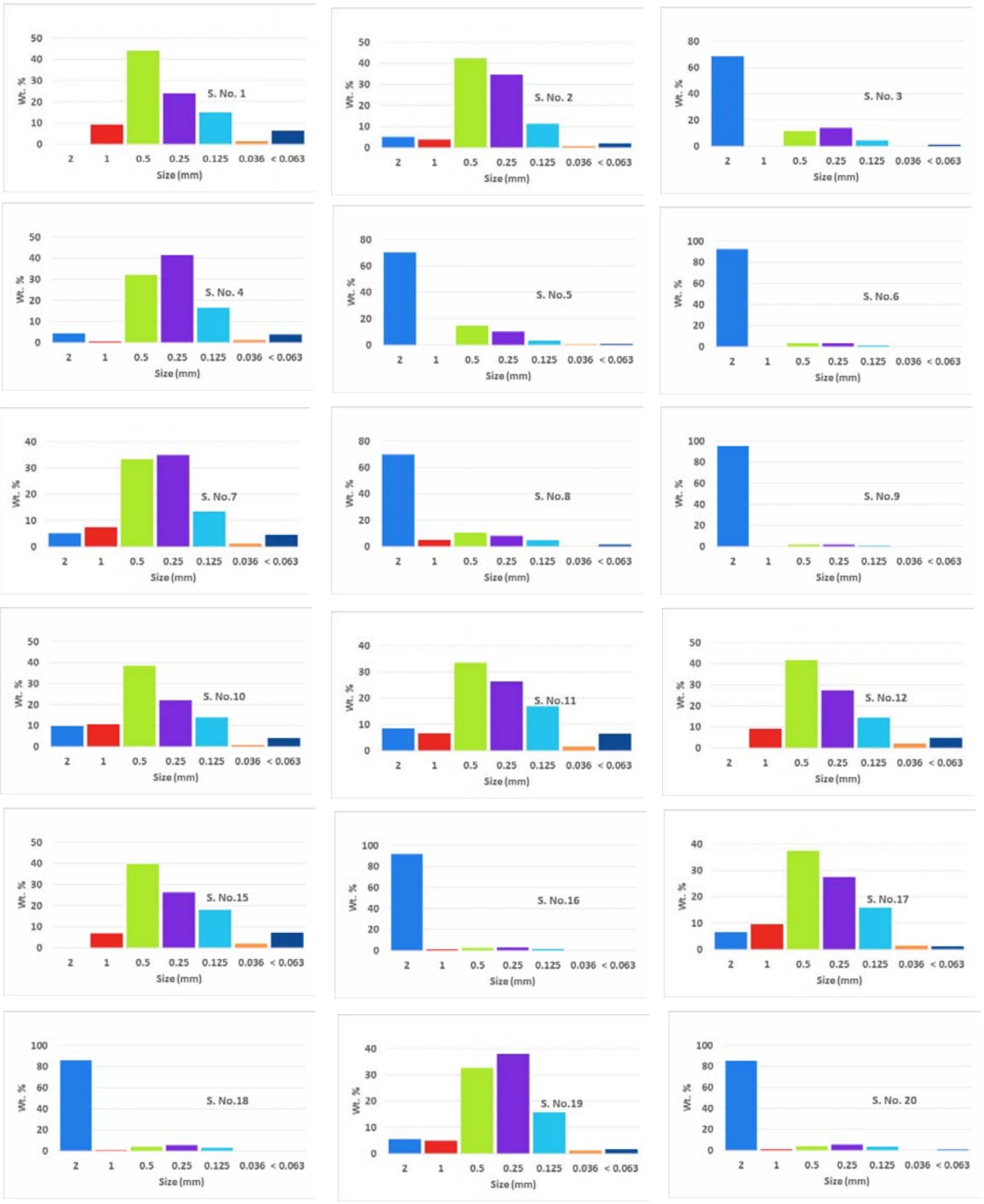

Fig. 8: Comparative histograms showing the grain size distribution of the studied samples.

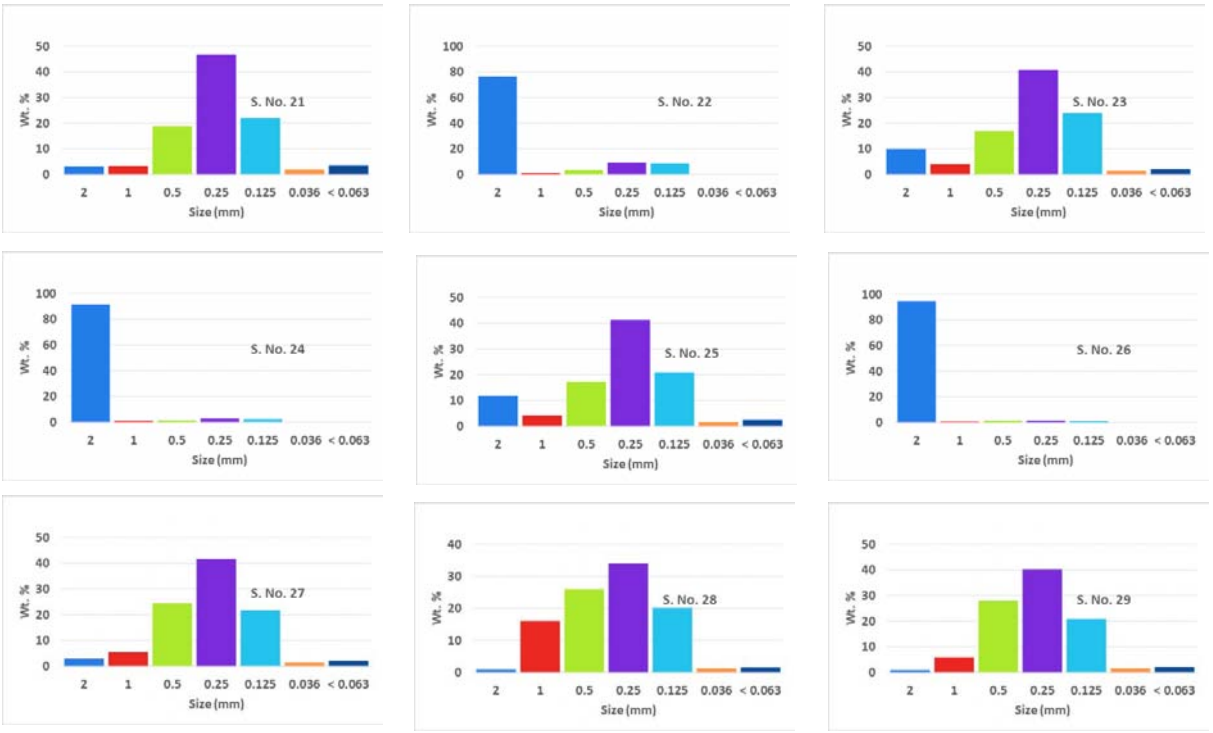

Fig. 8 (continued).

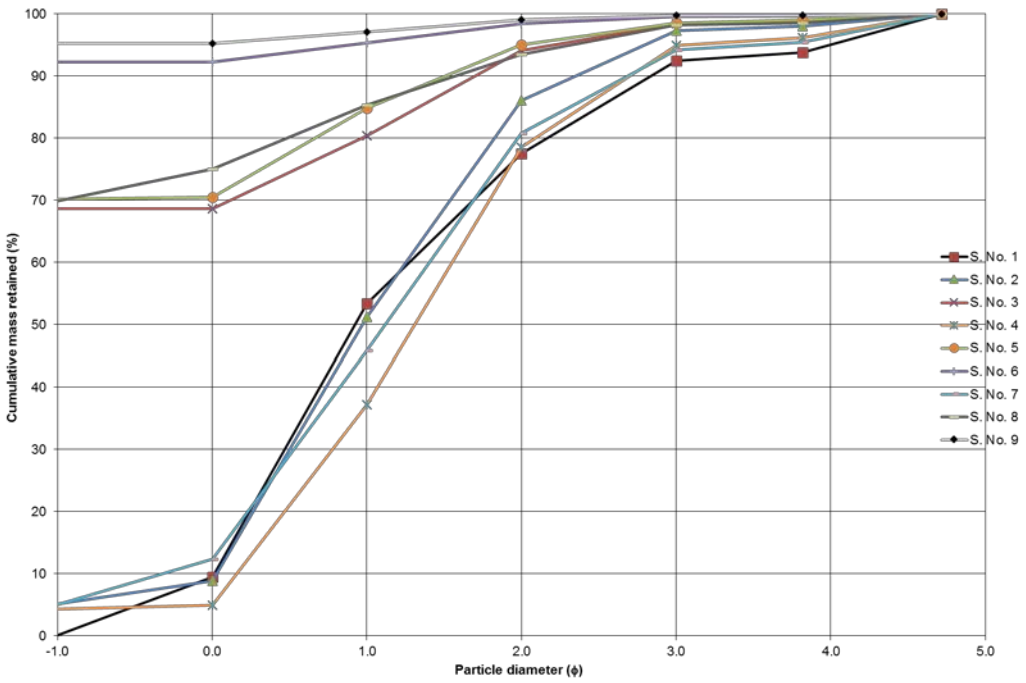

Fig. 9: Grain- size distribution cumulative curves (phi) of the studied samples.

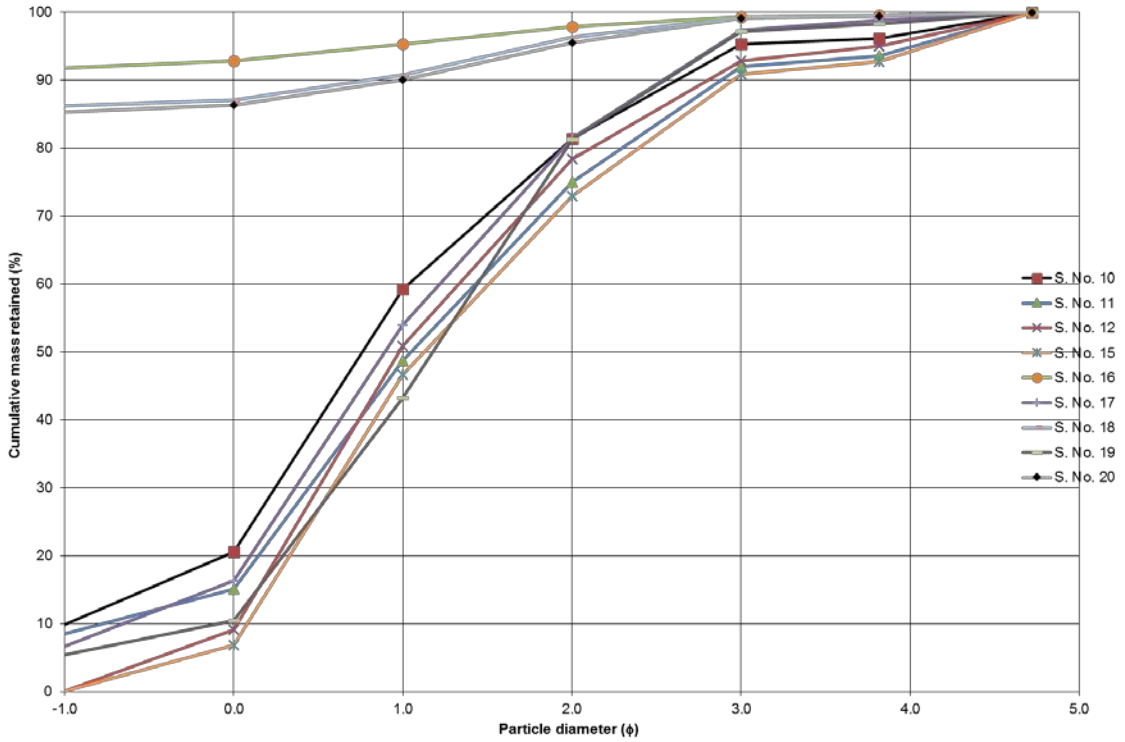

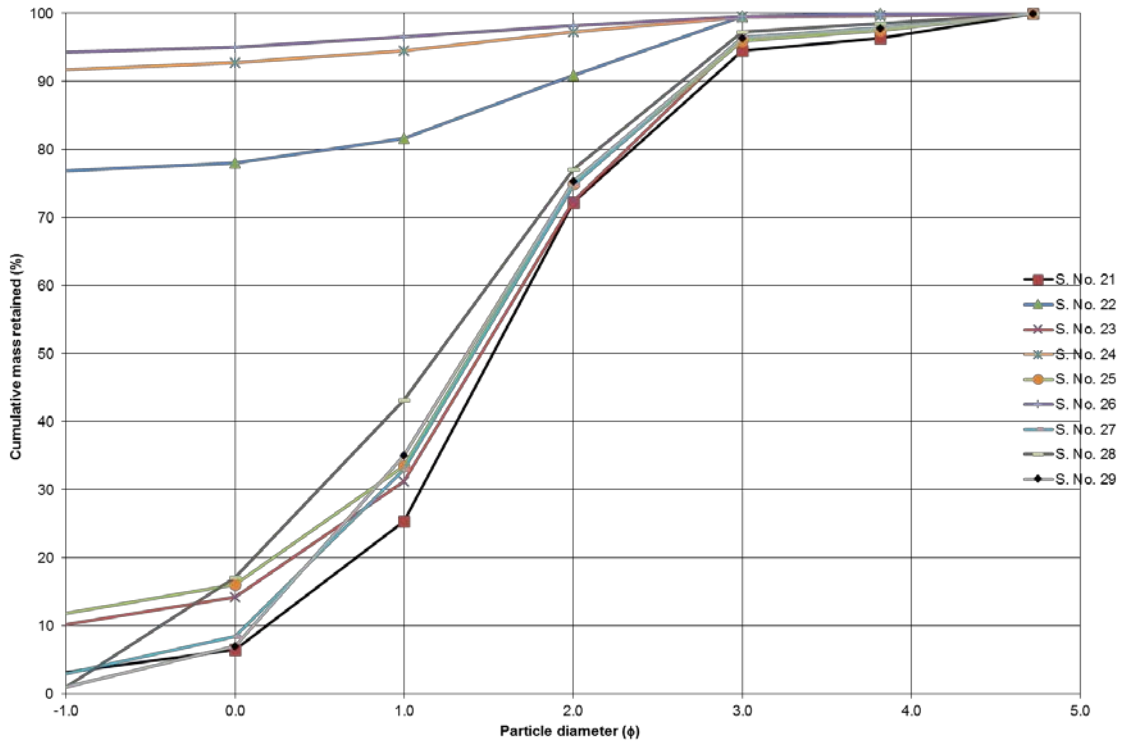

Fig. 9 (continued).

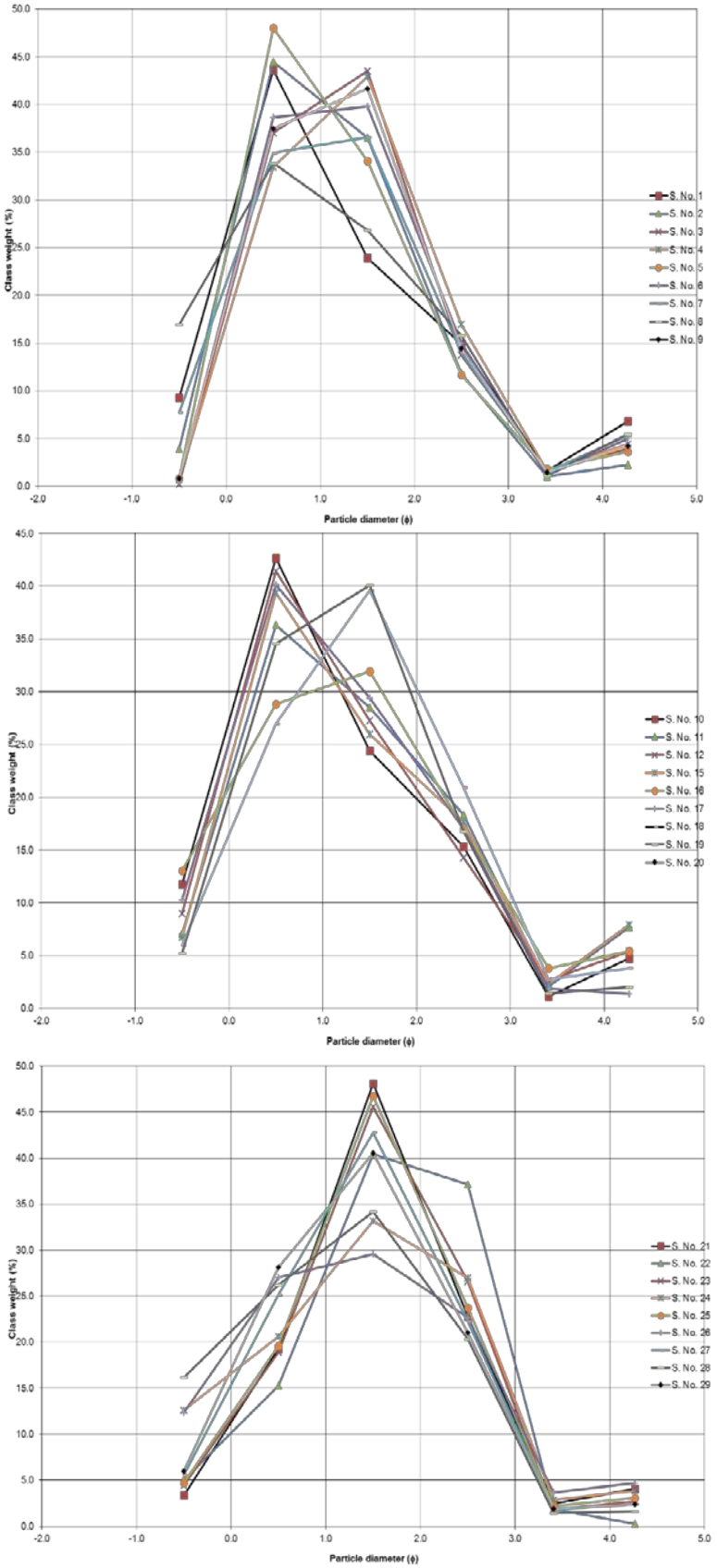

Fig. 10: Distribution curves (phi) of the studied samples.

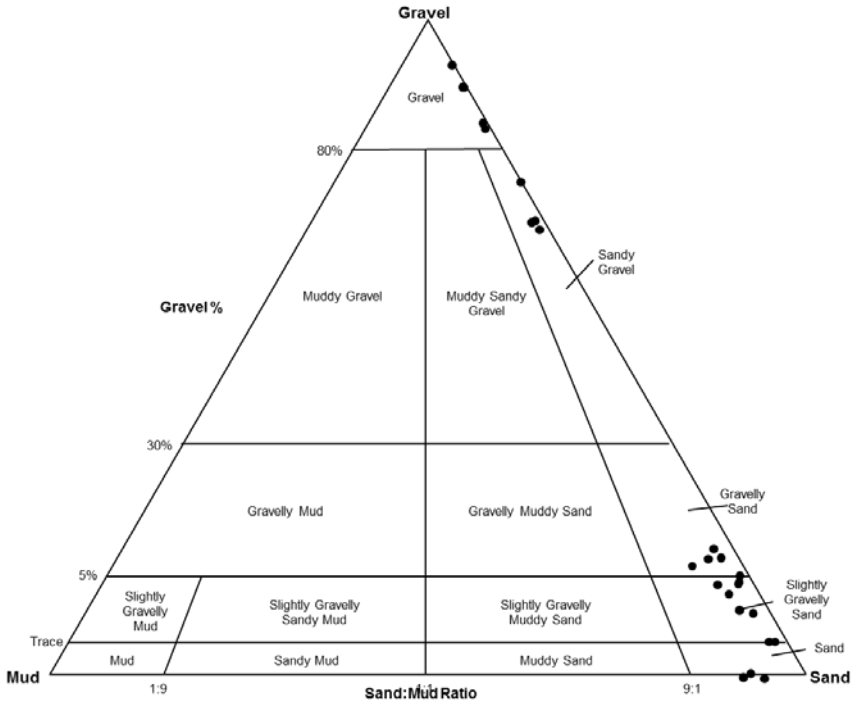

Fig. 11: Plots of the studied sand samples on Folk diagram (1954).

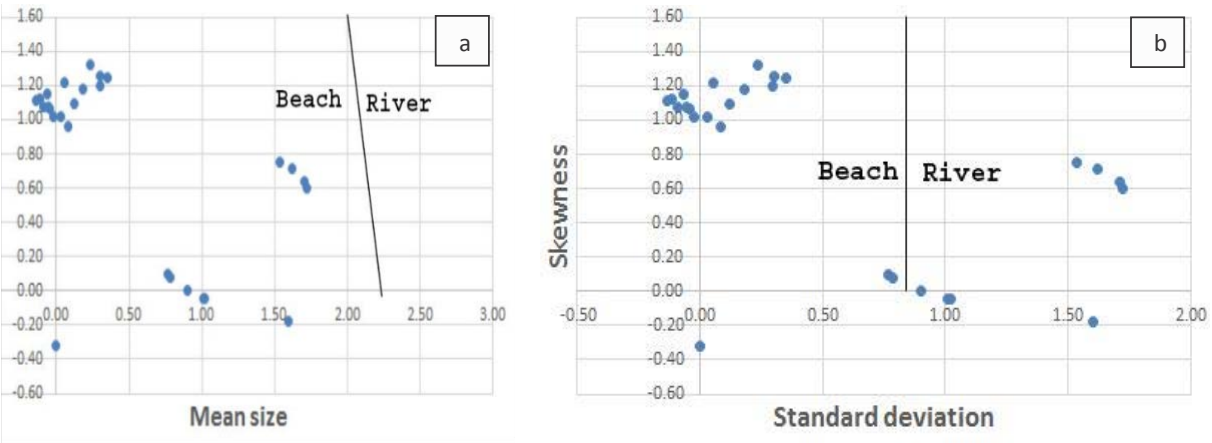

Fig. 12: Scatterplot for distinguishing between beach and river clastic sediments: a) plot of skewness versus mean size; b) plot of skewness versus standard deviation (Moiola and Weiser 1968).

b. Ferruginous quartz-wacke facies

Microscopically, the quartz wacke composed of detrital quartz grains (up to 65%), and lithoclasts (up to 5%) with iron oxides (up to 30%). The quartz grains are mainly of sub-angular to sub-rounded, medium to coarse in size, moderately/poorly sorted, quartz occurs both as monocrystalline and polycrystalline grains. The monocrystalline variety is much more abundant than the polycrystalline, most of the quartz grains show uniform extinction cemented with ferruginous material (Figs. 15& 16) and silica (Fig.17). The grains are not in contact but a few shows straight, concavo-convex and sutured contacts, many of the quartz have overgrowths around them with a fine line of iron oxide.

Most of the quartz grains are fresh and clean, while some of them are dirty and display shades of pale yellow to reddish colors due to the staining by ferruginous cementing material, some of the quartz grains show fractures, which are filled with cement or opaque material (Fig.14). The presence of ferruginous material in the form of cement is more abundant feature in thin sections of the Gabal Ahmar sandstone. The detrital quartz grains may appear to float in the ferruginous clay-like matrix and exhibit no point of grain contact and have low porosity, this low porosity is referred to iron oxides which are filled the pore spaces, as shown in (Figs. 15).

Adenes red pigment and the existence of fine quartz grains extensively corroded with ferruginous material. The grains are coated by a continuous red hematitic coatings urrounding the entire surface of the sand grains and sometimes entirely staining the quartz grain (Fig. 16).

c. Calcareous quartz-wacke facies

Calcareous quartz -wackes howing monocrystalline and polycrystalline quartz grains, rounded to sub-angular, with some grains showing evidence of embayment (monocrystalline quartz grain with observed embayment in micritic carbonates cement). Micrite and directional orientation sericite (Figs. 18&19) are the cement of some quartz-wacke facies; they are formed from the replacement or alteration of feldspar. Elongated mica flakes and fine line show mechanical bending due to early compaction (Figs. 20&23). Ferruginous lithoclasts are present in some samples (Fig. 21) . The contacts between the sub-grains are straight to suture, the latter occurs more commonly, the quartz grains are cemented by non-ferroan sparry calcite (Fig. 22).

Several theories concerned with the origin of carbonate cement in sandstones are discussed in Pettijohn et al., (1972). A late secondary origin is suggested for the calcite cement in the Gabal Ahmar sandstones from the evidence of its corrosive effect on the detrital quartz overgrowth. Although there is no clear evidence for the ultimate source of the cementing carbonate, there appear to be one possibility: the carbonate is derived from adjacent Eocene carbonate formations (i.e. Observatory, El-Qurn, Wadi Garawi and Wadi Hof), by leaching and circulating groundwater.

The dissolved carbonates are redistributed, initially as pore fillings, and in some places concentrated to such a degree that marginal replacement of adjacent detrital grains is ensured. Although the studied thin section has shown that there is no obvious vertical trend in carbonate cementation of the Gabal Ahmar sandstones, the absence of carbonate cement in some samples is frequently due to weathering and leaching processes.

The sandstone sequences have been subjected to several important diagenetic changes since their depositional history. Their paragenetic sequence begins with primary partial silica cementation, which was followed by formation of iron in the remaining pores. Both these stages involve quartz overgrowths produced as a result of pressure solution. Later stages proceeded by precipitation of carbonate in new pore spaces created by partial replacement and corrosion of detrital quartz grains.

From the petrographic studies it could be summarized that in general the quartz grains are monocrystalline with normal and wave extinction and polycrystalline with sutured and straight crystal boundaries, the presence of elongated in a preferred direction (stretched quartz), (Fig. 23), and the poorly sorting of the most sand samples, it can be concluded that the source of the studied sand is the igneous and metamorphic rock of the North Eastern Desert.

4.2.2Mineralogical Investigation

4.2.2.1Mineralogy of the bulk sediments

The X-ray diffractograms of the studied bulk samples (Fig. 24) cl early show t hat the G abal Ahmar sand and sandstone consist of (in descending order of abundance): quartz (38.8-95.4%), m ontmorillonite (8.9-27.3%), calcite (3.9-23.4%), m icrocline (12%) a nd he matite (3.8-10.4%).

4.2.2.2 Heavy mineral analyses

The he avy minerals present i n t he s tudied sample with specific gravity > 2.85g/cm3 were allowed to settle to the bottom of the separating funnel or after which the filtrate (heavy mineral) were thoroughly washed with acetone to remove any trace of bromoform and also dry. The different recorded heavy minerals assemblages in the studied sand samples can be classified into two opaque and non-opaque mineral groups (Folk (1980).

Identification of minerals

The w eight de nsity a nd concentrations of light m inerals, m agnetic a nd non -magnetic heavy minerals are shown in table 2.

A- Light minerals

The light minerals were concentrated first forming t he p remier o f f ractions. Q uartz i s the main light minerals, which form content up to 98.93% of samples and calcite also is present in some samples in a small amount reached to 2%. Quartz is generally represented by fine to very fine grained, angular to sub-angular and yet sub-rounded grains, colorless, reddish and yellowish (Figs. 25a, b & c). While the calcite is present in the form of colorless a nd reddish (stained w ith hematite) flaks.

B- Heavy minerals

The heavy minerals are divided into magnetic (constitute 67.3% (fine fraction) and 64.5% (very fine fraction) on the average) and non-magnetic minerals (constitute 32.4% (fine fraction) and 35.3% (very fine fraction) on the average). The magnetic minerals are represented only by magnetite. On the other hand, the non-magnetic minerals are divided into metallic and non- metallic minerals. The m etallic minerals comprise he - matite a nd l imonite. However, the non -metallic minerals are represented by zircon, with addition to glauconite. All the identified grains of heavy minerals show di fferent shapes l ike euhedral t o anhedral, angular to sub angular and rounded to sub-rounded shape.

a. Magnetic heavy minerals

The m agnetic m inerals ar e r epresented by homogenous (Fig. 26b) and heterogeneous magnetite. T he latter is usually associated with hematite and limonite as inclusions or intergrowth (Figs.29a&c). T he magnetic minerals are represented by hom ogenous m agnetite g rains, as well as grains composed of different minerals as inclusions. Magnetite w as recorded in all st udied samples, forming an amount varying from 23.4% to 98.5% (Tab.2). Magnetite displays as deep reddish b rown to b lack c olor a nd w ith metallic to dull lus ter, s ometimes w ith r eddish brown color, probably due to hematization, their habit ranges from massive, granular and angular to sub-angular grains.

b. Non-magnetic heavy minerals

The petrographic study of non-opaque transparent heavy minerals separated from fine and very fine-grained sands, the presence of hematite, limonite, zircon and glauconite was verified in all samples analyzed.

The he matite is represented by hom ogenous (Fig.26a) and heterogeneous us ually assoc iated with quartz, magnetite a nd limonite a s in clusions or i ntergrowth (Figs.25b, 29a, b& e). He-matite constitutes content varying from 3.7% to 62.5% of heavy minerals. It occurs as angular to sub-rounded d eep red t o pu ffery r ed colored grain.

The limonite minerals are represented by homogenous (Fig. 26c) and heterogeneous hematite us ually a ssociated w ith qua rtz, magnetite and hematite as i nclusions o r intergrowths (Figs. 25c, 29b& c). L imonite constitutes content varying from 1.2% to 49.2% of heavy minerals. It occurs as vary size, angular to sub-rounded deep t o pa le yellow colored grain.

Zircon is detected in many samples with content varying from 0.41 to 8.5%. Their color varies from colorless, pale yellow, reddish brown, brownish and yellowish red color with inclusion. Zircon is often represented by short to long prismatic form euhedral to subhedral shape with pyramid termination, rounding of the edges of the zircon grains is relatively not detected. Most of the transparent grains usually have homogenous compositions; the other colored grains have some inclusions such as grains of yellow and red colors (Figs. 28 and 29d). As mentioned by Dill et al. 2008, zircon is common as accessory minerals in acidic igneous rocks

Glauconite is detected in many samples with content varying from 1.5 to 11.2%. It occurs as angular to sub-rounded grains varying in color from green to pale green (homogeneous), (Fig. 27) and reddish green color with inclusion (heterogeneous), (Fig. 29e).

In grain-size distributions magnetic and non-magnetic heavy minerals in sand sediments, zircon and glauconite are present in higher frequencies in very fine-grained sands, (Tab. 2), due to differences in the specific gravities of these minerals (Tucker, 2001). Their hesitations are higher in very fine sands than in fine-grained sands.

4.3 Geochemical investigation

The major and trace element concentrations of the Gabal Ahmar sandstones are listed in Tables 3 and 4. The result of the chemical analysis indicates that the sandstone exhibits high SiO_2 contents ranging from 29.61 to 91.74% with an average value of 73.39% while alumina (Al_2O_3) contents range between 2.70% and 6.00% with an average of 3.73%. The sandstone is therefore highly siliceous, with exception of three calcareous sandstone samples which record high con- tents of CaO up to30.35%. Low alumina might be indicative of the dearth of alumino-silicate minerals in the provenance.

Generally, SiO_2 and Al_2O_3 constitute 93.81% of the entire composition (seven samples) indicating that the sandstone is chemically mature, probably as a result of its enriched chemically stable minerals. The studied samples contain small amount of Na_2O (0.17- 0.47%) with an average of (0.27 %).

The depletion of Na2O (<1%) in sandstones can be attributed to a relatively smaller amount of Na-rich plagioclase in them, consistent with the petrographic data. It shows negative correlation with K_2O (r= -0.78), (Fig. 30). The maximum value of K_2O is 0.2 wt% with the average value of 0.19 wt%., Sodium and potassium present in some samples in the form of sericite cement.

CaO content varies from 0.30 wt% to 30.35 wt% with average content of 8.95 wt%. MgO occurs in minor amount, and show minimum value of 0.5 wt% and maximum value of 1.74 wt% with an average content of MgO is 0.88 wt%. The higher concentration of TiO_2 (average 0.36 wt %) suggest that the sediments were subjected to intensive weathering in the source area (Roy et al., 2007).

In general, SiO_2 increases and TiO_2, Al_2O_3, Fe_2O_3, MnO, CaO, MgO and K_2O decrease (r= -0.98, -0.99, -0.99, -0.74, -0.9, -0.99 and -087 respectively) in the studied samples, it is attributed to the increase in mineralogical maturity.

One interesting feature of the correlation matrix is the strong negative (r=-0.99) of correlation between SiO_2 and Al_2O_3 indicating that much of the SiO2 is not associated with the Al_2O_3. This is probably due to the fact that much of the SiO_2 is present as quartz grains (Ogala et al., 2009 and Prachiti et al., 2011), and the minor role of clay fraction appears in the sandstones on the major oxide abundance (Ahmad et al., 2014).

Fe_2O_3 content is on the average 3.09%. The Higher content of iron may be related to the abundance of iron oxide heavy minerals (magnetite, hematite and limonite) and partly to Fe- containing clay minerals. Fe_2O_3 shows a strong positive correlation with MgO and Al_2O_3 (r= 0.98 and 0.98), (Fig.30). With respect to the linear correlation (Fig.30) for the major and trace elements, the positive correlation between TiO_2 and the elements Zr and Zn (r=0.23and 0.58), (Fig. 30) in the secondary environment shows that these elements come from very resistant minerals such as zircon.

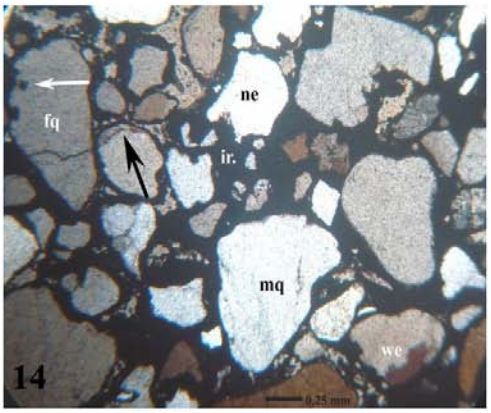

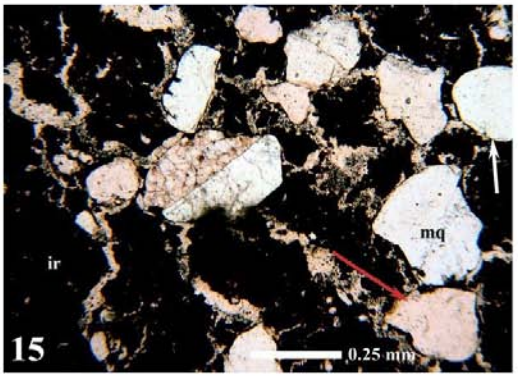

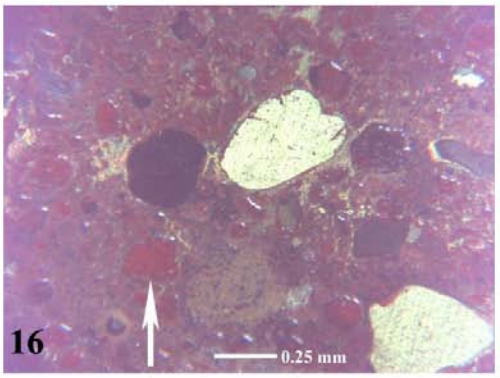

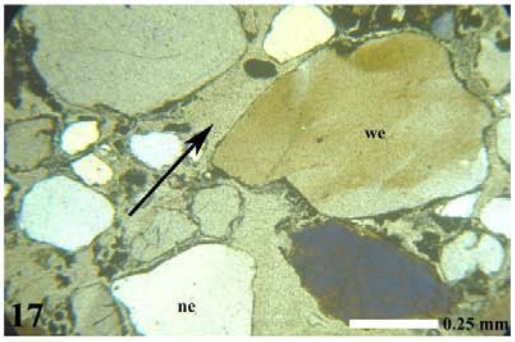

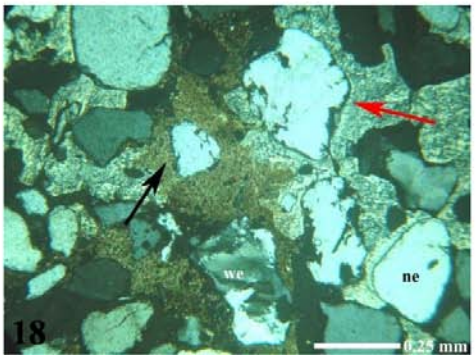

Fig. 13: a) photograph showing fractured gravels staining with iron oxides, b): showing different shape and size of gravels. Fig. 14: Photomicrograph showing ferruginous sandstone, the quartz grains are fine to coarse, monocrystalline quartz (mq) with normal (ne) and wave extinction (we) sub-angular to sub-rounded, poorly sorted, some fractured quartz grains (fq) iron oxides (ir) is present as cement and inclusion in fractures (arrows).

Fig. 15: Photomicrograph showing ferruginous-wacke, the grains are of monocrystalline (mq) clean (white arrow) and stained (red arrow) and sub-angular to sub-rounded (white arrow) the grains are not in contact but a few show straight contacts, many of the quartz have overgrowths around them with a fine line of iron oxide iron oxides (ir) is present as cement.

Fig. 16: Photomicrograph showing ferruginous-wacke, the grains are of monocrystalline and sub-rounded and normal extinction and some grains are entirely stained with iron oxides. (white arrow)

Fig. 17: Photomicrograph showing sub-angular to sub-rounded, fine to coarse in size, poorly sorted, quartz occurs both as monocrystalline with normal (ne) and wave (we) extinction the quartz grains are cemented by silica (black arrow).

Fig. 18: Photomicrograph showing monocrystalline quartz grains with normal (ne) and wave extinction embayment in micritic carbonates cement (black arrow) and directional orientation sericite cement (red arrow).

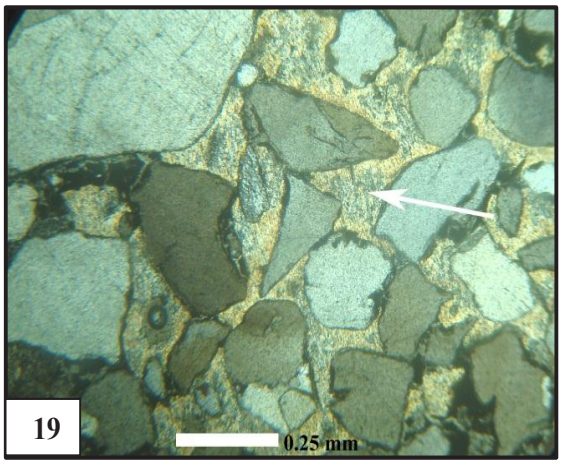

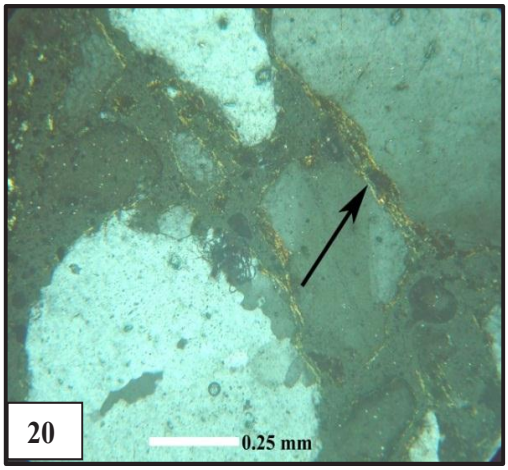

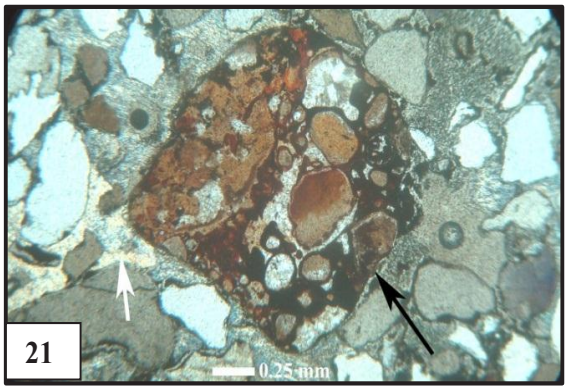

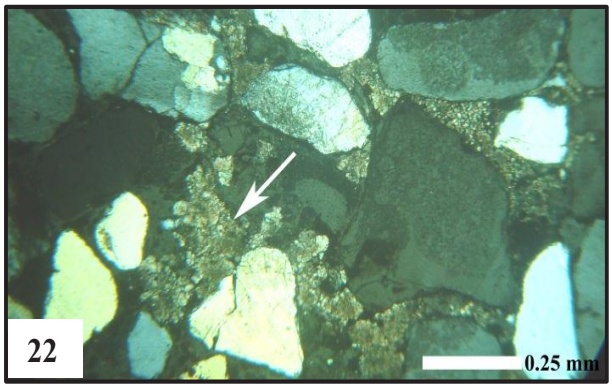

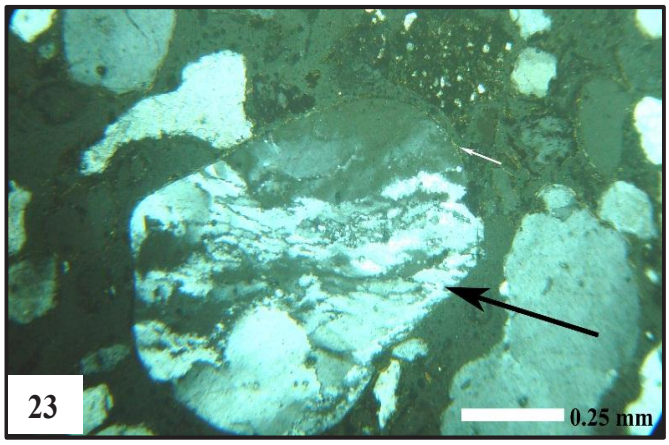

Fig. 19: Photomicrograph showing directional orientation sericite cement (white arrow).

Fig. 20: Thin section image showing a twisted and fine line mica (black arrow) between the quartz grains.

Fig. 21: Photomicrograph showing ferruginous lithoclasts (black arrow).

Fig. 22: Photomicrograph of calcareous quartz -wacke showing monocrystalline and polycrystalline, rounded to sub-angular quartz grains. The contacts between the sub-grains are straight to suture, the latter occurs more commonly, the quartz grains are cemented by non-ferroan sparry calcite (white arrow).

Fig. 23: Photomicrograph showing stretched quartz grain (black arrow) and a fine line of mica (white arrow).

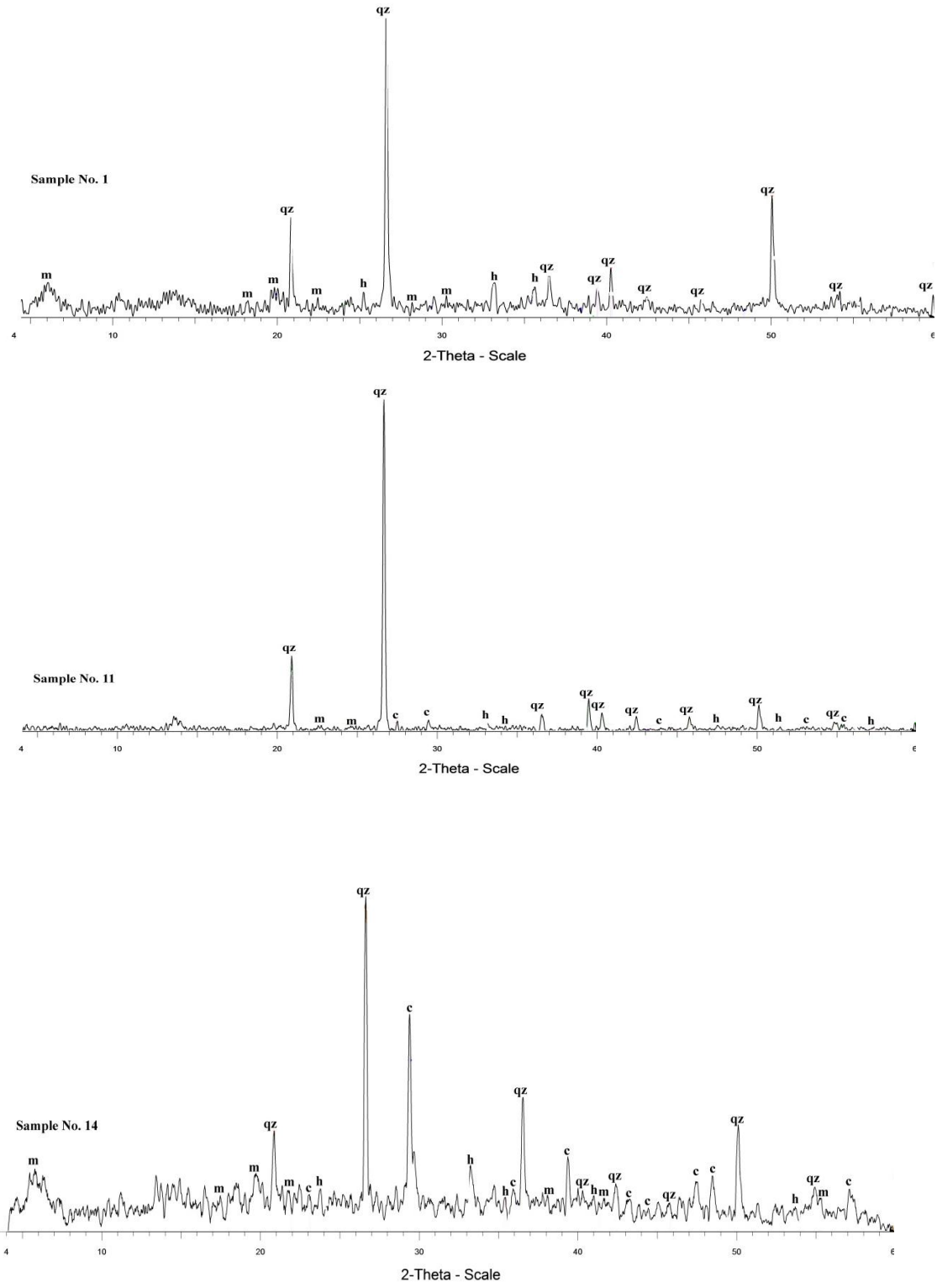

Fig. 24: Representative profiles of X-ray diffraction patterns for three selected samples, where; qz: quartz, c: calcite, h: hematite, and m: montmorillonite.

Table (2) Weight and density of the investigated sand samples

S. No.	Size (mm)	Wt. (gm)	Wt. of light minerals		Wt. of heavy minerals							
			(gm)	(%)	Magnetic (%)	Non- magnetic (%)				Total wt. of Non-magnetic (%)	Total wt. of heavy minerals	
						H	L	Z	G		(gm)	(%)
2	0.125	10.00	9.08	90.80	60.5	37.3	0	0.41	1.65	39.3	0.92	9.20
	0.071	3.35	3.30	98.51	38.7	54.2	0	4.6	2.3	61.1	0.05	1.49
5	0.125	10.00	9.69	96.90	80	16.6	0	0	3.3	19.9	0.31	3.10
	0.071	7.98	7.81	97.87	63.8	31.9	0	0	4.2	36.1	0.17	2.13
9	0.125	10.00	9.78	97.80	50	43.6	0	1.7	4.6	49.9	0.22	2.20
	0.071	1.87	1.85	98.93	71.4	26.1	0	0.79	1.5	28.47	0.022	1.18
10	0.125	10.00	9.75	97.50	66.81	26.8	0	0.51	5.1	32.4	0.25	2.50
	0.071	4.08	3.97	97.30	67.4	22.4	0	3.3	6.7	32.4	0.097	2.38
12	0.125	10.00	9.67	96.70	66.2	16.8	1.2	4.49	11.2	33.69	0.26	2.60
	0.071	10.00	9.73	97.30	58.8	25.7	0	5.51	9.9	41.11	0.27	2.70
16	0.125	10.00	8.99	89.90	51.3	0	48.7	0	0	48.7	1.1	11.00
	0.071	6.51	4.46	68.51	50.8	0	49.2	0	0	49.2	2.09	32.10
17	0.125	10.00	9.91	99.10	93.5	0	3.8	2.5	0	6.3	0.09	0.90
	0.071	7.24	7.19	99.31	87.71	0	0	10.5	1.75	12.25	0.05	0.69
21	0.125	10.00	9.92	99.20	83.3	12.9	1.85	1.85	0	16.6	0.08	0.80
	0.071	10.00	9.77	97.70	91.7	0	3.0	4.5	0.61	8.11	0.23	2.30
25	0.125	10.00	9.93	99.30	23.4	62.5	7.8	4.6	1.5	76.4	0.07	0.70
	0.071	7.96	7.94	99.75	25.6	59.8	0	8.5	5.9	74.2	0.02	0.25
29	0.125	10.00	9.85	98.50	98.5	1.4	0	0	0	1.4	0.21	2.10
	0.071	7.67	7.54	98.31	89.2	3.7	0	7	0	10.7	0.13	1.69

H: Hematite L: limonite Z: zircon G: glauconite

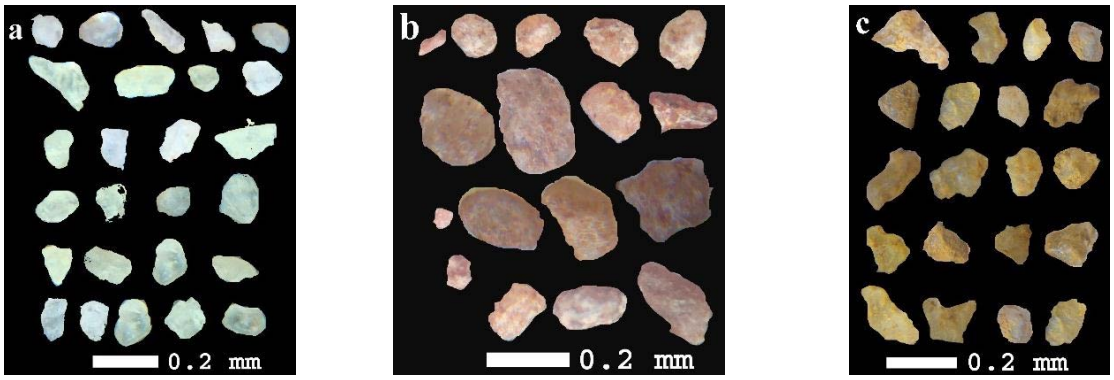

Fig. 25: Photomicrograph showing angular and sub rounded grains of; light quartz (a), hematitic (b) and limonitic quartz (c).

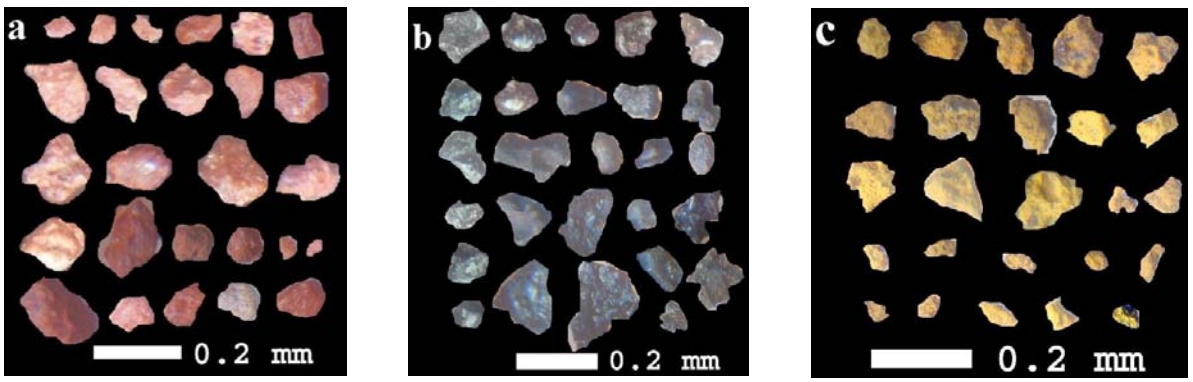

Fig. 26: Photomicrograph showing different types of angular and sub rounded grains of homogenous iron oxides; (a), hematite, (b) magnetite and (c) limonite.

Fig. 27: Photomicrograph showing angular and sub rounded grains of homogenous glauconite.

Fig. 28: Photomicrograph of prismatic zircon grains.

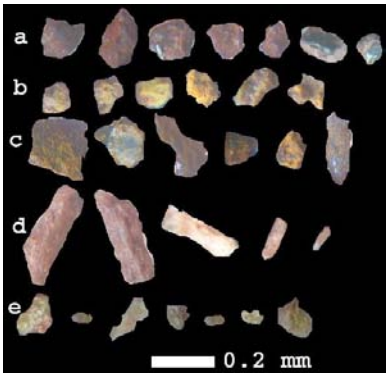

Fig. 29: Photomicrograph showing different inclusions; hematite- magnetite (a), hematite- limonite (b), magnetite-limonite (c), zircon-hematite (d) and glauconite- hematite grains (e).

Table (3): Representative chemical analyses (wt %) of sandstones from the Gabal Ahmar Formation in the study area.

S. No.	SiO_2	Al_2O_3	Fe_2O_3	MgO	CaO	Na_2O	K_2O	MnO	TiO_2	P_2O_5	SO_3	H_2O
7	91.74	2.90	2.27	1356	0.36	0.23	0.20	0.038	0.17	0.095	0.04	1335
8	90.82	3.00	2.20	0.51	0.40	0.22	0.21	0.10	0.21	0.11	0.054	2.01
10	33.30	5.50	5.37	1.58	26.76	0.47	0.18	13125	0.69	0.19	0.13	25334
13	29361	6311	4396	1373	29371	1341	1312	1331	1385	1319	1316	25383
14	91371	2381	2.20	1362	0.30	0.20	0.23	0.043	0.13	0.090	0.08	2335
16	91381	3317	2317	1355	1344	1317	1324	1311	1324	1311	1315	2311
18	91.80	2.79	2.30	0.50	0.30	0.20	0.22	0.12	0.21	0.10	0.004	1.35
22	34.50	5.60	5.11	1.74	30.35	0.40	0.11	0.46	0.84	0.18	0.082	26.02
25	90.30	2.70	2.17	0.55	0.45	0.20	0.20	0.15	0.18	0.08	0.054	2.20
28	90.40	2.90	2.21	0.50	0.47	0.25	0.24	0.13	0.17	0.09	0.050	1.30
Ave.	**73.39**	**3.72**	**3.09**	**0.88**	**8.95**	**0.27**	**0.19**	**0.14**	**0.36**	**0.12**	**0.06**	**8.97**

Table (4): Trace elements analyses (ppm) of sandstones from the Gabal Ahmar Formation in the study area

S. No.	Co	Ni	Cu	Zn	As	Sr	Y	Zr	Nb	Ba	Cr	Rb
7	ND	27	23	35	ND	41	ND	111	ND	90	45	6
8	41	39	31	35	ND	33	10	129	12	123	49	ND
10	85	62	36	54	ND	379	25	150	14	39	47	ND
13	69	56	44	47	5	211	32	129	12	238	ND	ND
14	ND	28	24	36	ND	42	ND	113	ND	92	46	6
16	41	41	34	66	ND	36	11	196	ND	133	ND	ND
18	40	27	26	20	ND	34	37	120	12	101	40	5
22	ND	50	35	38	6	388	40	170	ND	233	49	ND
25	35	36	34	35	ND	33	ND	173	15	139	ND	ND
28	ND	27	25	40	ND	35	15	135	ND	120	51	ND
Ave.	**31.1**	**39.3**	**31.2**	**35.9**	**1.1**	**123.2**	**16.9**	**142.6**	**6.5**	**130.9**	**32.7**	**1.7**

Table (5): Classification of the studied samples.

Samples	Log SiO_2/Al_2O_3	Log K_2O/Na_2O	Classification of sandstone type
7	1.49	-0.06	Greywacke
8	1.48	-0.02	Greywacke
10	0.78	-0.41	Greywacke
13	0.69	-0.53	Greywacke
14	1.5	0.06	Arenite
16	1.5	-0.14	Greywacke
18	1.51	0.04	Arenite
22	0.78	-0.56	Greywacke
25	1.52	0	Arenite
28	1.49	-0.01	Greywacke

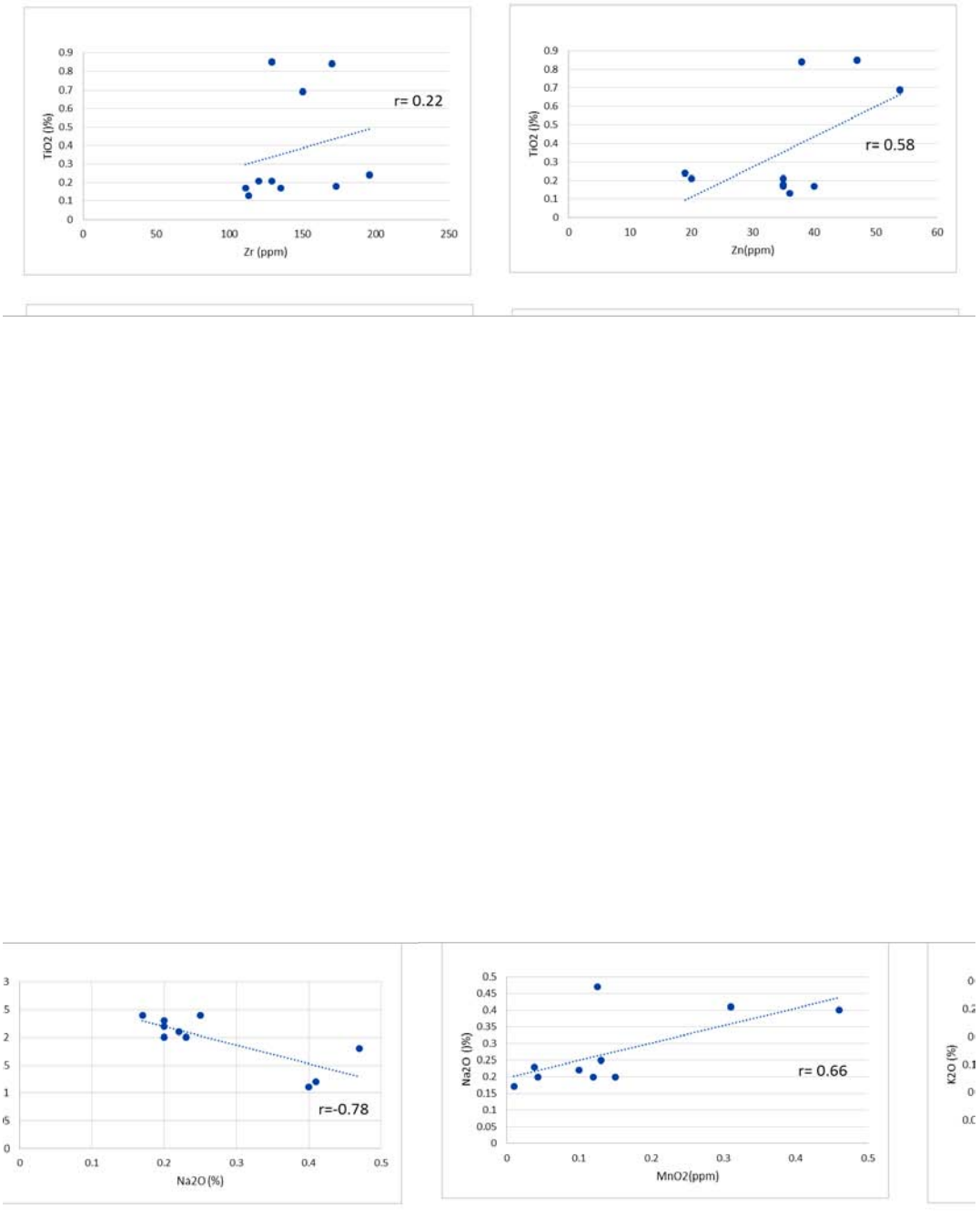

Fig. 30: Correlation between major (in %) and trace elements (in ppm) in the studied sandstone samples.

Generally, the positive correlation of Na with Mn (0.66), (Fig. 30) suggests terrestrial origin of Na. Also, the nearly homogenous concentrations of Na and K in the sediments simply refer to single dominant source (Mansour et al., 2013).

Also, the enrichment of Zr, in these sediments which are high field strength elements indicates their source rock could be granitic. The strong positive correlation of Zn with several other elements (Fig. 30) may be due to the zircon is highly mobile and is also naturally abundant in the crust and in sedimentary rocks.

The positive correlation between iron and Mg, Ni, and Zn (r=0.98, 0.89 and 0.68) is due to its relationship with the ferromagnesian minerals supplied by the terrigenous materials (Roy and Roser 2012).

The negative correlation of Mg with K (r=-0.89) and the positive correlation with Co (Fig. 30) as well as Ni (r=0.87 and 0.93) may be attributed to the source of terrigenous clays and suggests their transport to the marine environment across landfill (Rao et al. 2002). Mn shows positive correlations with Na (0.66) and negative correlation with total carbonate, which reveals that the occurrence of manganese in oxide form in the marine environment is more remarkable than its occurrence in the carbonate forms, reflecting naturally terrigenous origin for Mn (Roy and Roser 2012). The relatively increase in Zn content of the studied sediments may be due to the influence of Zn-rich terrigenous fragments.

The Sr content (33—388 ppm) of the studied sandstones is variable; this variability is caused by many influences on Sr in low temperature depositional environments (Fairbridge 1972). For instance, the distribution of Sr can be affected by the presence of Ca(r=0.93), (Fig.30), fractionation of Sr can result from the weathering of feldspars, particularly plagioclase, and additional Sr can be incorporated in diagenetic carbonate, as also noticed in the studied sandstones (Vdacny et al., 2013).

The geochemistry of the studied sandstones supports the petrographic results. The Gabal Ahmar sandstones are geochemically classified using Blatt et al., 1972; Herron, 1988 and Pettijohn, 1972 into arenite and greywacke and based on the calcium content the sandstones are non-calcareous into non-calcareous (Ca < 4 %), calcareous (4 % < Ca < 15 %).

The concentrations of two major oxide groups has been used to classify sandstones (Tab. 5); silica and alumna and alkali oxides. The enrichment of SiO2 over Al2O3 by mechanical and chemical process produces quartz arenite, silica (quartz) enrichment is a measure of sandstone maturity, and is a reflection of the duration and intensity of weathering and destruction of other mineral during transportation.

CONCLUSIONS

The studied samples could be classified into three types, gravelly and slightly gravel sand, gravel and sand gravel and sand class. It is clear from the reprehensive histograms that the examined grain-size is related to unimodal and bimodal type samples, meanwhile the majorities are unimodal. Bivariate plots of the studied samples indicate that most of the samples falls in the field of beach while others within the field of fluvial environment, reveals that these sediments were deposited under diverse conditions by different process.

The petrographic investigation of the Gabal Ahmar sandstones indicates that they are mainly ferruginous arenite, ferruginous and calcareous greywackes. Mineralogically, quartz, montmorillonite, calcite, microcline and hematite are the main constituent (in descending order of abundance).

The heavy minerals are divided into magnetic and non-magnetic minerals. The magnetic minerals are represented mainly by magnetite, while the non-magnetic minerals are divided into metallic (hematite and limonite) and non- metallic minerals (zircon and glauconite).

Based on the geochemical data, the sandstones are calcareous and non-calcareous. Generally SiO_2 and Al_2O_3 constitute 93.81% of the entire composition (seven samples) indicating that the sandstone is chemically mature, probably as a result of its enriched chemically stable minerals.

REFERENCES

Ahmad, A. H. Noufal, K. N. Masroor, Alam, M. and Tavheed K. (2014): Petrography and geochemistry of Jumara Dome sediments, Kachchh Basin: Implications for provenance, tectonic setting and weathering intensity. Chin.J.Geochem., V. 33: p. 9–23.

Amaral, E. J. and Pryor, W. A. (1977): Depositional environment of the St. Peter sandstone deduced by textural analysis. J. Sed. Pet., V. 47: p. 32-52.

Balsinha M. Fernandes C. Oliveira A. Rodrigues A. and Tabor- da R. (2014): Sediment transport patterns on the Estremadura S pur co ntinental shelf: I nsights f rom grain- size trend analysis. J. of Sea Research, V. 93: p. 28-32.

Blair, T. B. McPherson, J. G. (1999): Grain-size and textural classification of coarse sedimentary particles. J. of Sedimentary Research, V. 69, p. 6–19.

Blatt, H. Middleton, G. and Murray, R. (1972): Origin of sedimentary rocks. Englewood Cliffs, New Jersey, Prentice-Hall, 634 pp.

Blott, S. J. and Pye, K. (2001): GRADISTAT: a grain size distribution and statistics package for the analysis of unconsolidated sediments. Earth Surface Processes and Landforms, V. 26, p. 1237-1248.

Dill, H. G. Techmer, A. Weber, B. and Fuessl M. (2008): Min- eralogical and chemical distribution patterns of placers and ferricretes in Quaternary sediments in SE Germa- ny: the impact of nature and man on the unroofing of pegmatites. J. Geochem. Explor., V. 96, p. 1–24.

Doeglas, D. J. (1946): Interpretation of the results of mechanical analysis. J. Sed. Pet., V.16, p. 13-40.

Folk R. L. (1980): Petrology of Sedimentary Rocks. Hemp- hill, Austin, 187pp.

Folk, R. L. and Ward, W. C. (1957): Brazos River bar: a study in the significance of grain size parameters. J. Sed. Pet., V. 27, p. 3–26.

Friedman, G. M. (1961): Distinction between Dune, Beach and River sands from their textural characteristics. J. Sed. Pet., V.31, p 514-529.

Friedman, G. M. (1967): Dynamic processes and statistical parameters compared for size frequency distribution of Beach and River sands. J. Sed. Pet., V. 37, p. 327-354.

Garwood J. C. Hill P. S. MacIntyre H. L. Law B. A. (2015): Grain sizes retained by diatom biofilms during erosion on tidal flats linked to bed sediment texture. Continental Shelf Research, V. 104: p. 37-44.

Herron, M. M., (1988): Geochemical classification of terrigenous sands and shales from core or log data: Journal of Sedimentary Petrology, V. 58, (5), p. 820-829.

Ingram, R. L. (1971): Sieve analysis. In: R.E. Carver (Ed.), Procedures in Sedimentary Petrology. Wilson Interscience, p.49-68.

Jitheshkumar, N. Rajganapathi, V. C. Sundararajan, M. Bhat K. H. and Velusamy S. (2013): Grain-size analysis and char- acterization of sedimentary environment a long O vari coast, Tamilnadu, India. International J. of Sediment Research.

Mansour A. M. Mohamed S. A. Hashem A. M. and Bakheit B. A. (2013): Assessment and comparison of heavy-metal co ncentrations in marine sediments in view of tourism activities in Hurghada area, northern Red Sea, Egypt. Egyptian Journal of Aquatic Research, V. 39, p. 91–103.

McLaren P. (1981): An interpretation of trends in grain size measurements. Journal of Sedimentary Petrology, V. 55: p. 457-470.

Moiola, R. J. & Weiser, D (1968): Textural parameters and evaluation. J. Sed. Pet, V. 38, p. 45-53.

Moss, A. J. (1962): The physical nature of common sand and pebbly deposits. Pt-1, Am. J. Sci., V. 261, P. 297- 343.

Moss, A. J. (1963): The physical nature of common sand pebbly deposits. Pt.2, Am. J. Sci., V. 261, p 297-343.

Moustafa, A. R. and Abd-Allah, A. M. A (1991): Structural setting of the central part of the Cairo- Suez district- Mid East Res. Cent., Ain Shams Univ., Sc. Res. Ser., V. 5, p. 133-145.

Nelson P.A. Bellugi D. Dietrich W. E. (2014): Delineation of river bed surface patches by clustering high-resolution spatial grain size data. Geomorphology, V. 205: p. 102-119.

Ogala, J. E. Ola-Buraimo A. O. and Akaegbobi, I. M. (2009): Palynological investigation of the Middle- Upper Maastrichtian Mamu Coal facies in Anambra Basin, Nigeria. World Applied Sciences J. V. 7(12): p. 1566-1575.

Ordóñez C. Ruiz-Barzola O. Sierra C. (2016): Sediment particle size distributions apportionment by means of functional cluster analysis (FCA). Catena V. 137: p. 31-36.

Pettijohn F. J. Potter P. E. Siever R. (1972): Sands and Sand- stones Springer-Verlag, New York, 618pp.

Pettijohn, F. J. (1975): Sedimentary Rocks, 3rd Edition, Harper and Row, New York.

Prachiti, P.K., Manikyamba, C., Singh, P.K., Balaram, V., Lakshminarayana, G., Raju, K., Singh, M.P.M., Kalpana, S., Arora, M., (2011): Geochemical systematics and Precious metal content of the sedimentary horizons of Lower Gondwanas from the Sattupalli coal field, Godavari Valley, India. International Journal of Coal Geology, V. 88, p. 83–100.

Roy, D. K. and Roser B. P. (2012): Geochemistry of Tertiary sequence in Shahbajpur-1 well, Hatia Trough, Bengal Basin, Bangladesh: Provenance, source weathering and province affinity. J. Life Earth Sci., V. 7: p. 1-13.

Roy, M. Tina van de F., Sidney R. H. and Steven L. G. (2007): 40Ar/39Ar ages of hornblende grains and bulk

Sm/Nd i sotopes of c ircum-Antarctic g lacio-marine sediments: Implications for sediment provenance in the Southern O cean. C hemical Geology V. 244, p. 507–519.

Said, R. (1962): The Geology of Egypt. Elsevier, Amsterdam-New York, 557pp.

Sharda, Y. P. and Verma, V. K. (1977): Paleo environment during M uree an d S iwalik sedimentation around U dhampur, Jammy Himalaya. Publication of the center of advanced study in Geology No. II, Punjab University, Chandigarh.

Shau, B. K. (1964): Depositional mechanisms from the size analysis of clastic sediments. J. Sed. Petrology, V. 34, 73-83P.

Srivastava, A. K. and Mankar, R.S. (2009): Grain size anal- ysis and depositional pattern of upper Gondwana sedi- ments (Early Cretaceous) of Salbardi area, Amravati d istrict, Maharashtra and B etul, Madhya Pradesh. J. Geol. Soc. India, V.73, p.393-406.

Temitope D. an d Timothy O. (2016); Sediment Characterisation in an Estuary - Beach System. J. Coast Zone Manag, V. 19 Issue 3.

Thokchom D. D. (2014): Textural characteristics and depositional environment of olistostromal sandstone of Ukhrul, M anipur. International Journal of R ecent D evelopment in Engineering and Technology V. 2, Issue 1.

Tucker, M . E. (2001): Sedimentary pe trology. B lackwell, Oxford, 262 pp.

Vandenberghe J. (2013): Grain size of fine-grained windblown sediment: a powerful proxy for process identification. Earth-Sci Rev V. 121: p. 18-30.

VĎAČNÝ, M. VOZÁROVÁ, A. and VOZÁR, J. (2013): Geochemistry o f t he Permian s andstones f rom t he Malužiná F ormation i n t he M aléKarpatyMts (Hronic Unit, Western Carpathians, Slovakia): implications for source-area weathering, p rovenance an d t ectonic s etting. Geologica Carpathic, Feb. V. 64, (1), p. 23—38.

Visher, G.S. (1969): Grain size distribution and depositional process, Jour. Geol V.39, p. 1074-1106.

Zingg, Th. (1935): Beiträgezur Schotteranalyse: Min. Petrog. Mitt. Schweiz., V. 15: p. 39-140.